Article:
Wang, Q, Zhu, B, Shen, J et al. (3 more authors) (2022) Quantifying Controls on Threshold Pressure during CO_2 Injection in Tight Gas Reservoir Rocks. Energy and Fuels, 36 (12). pp. 6292-6304. ISSN 0887-0624

https://doi.org/10.1021/acs.energyfuels.2c01307

Quantifying controls on threshold pressure during CO_2 injection in tight gas reservoir rocks

Wang Qian[1], Shen Jian[1], Paul W.J. Glover[2], Piroska Lorinczi[2], Lu Zhao[3]

1 School of Resources and Geosciences, China University of Mining and Technology, Xuzhou, 221000
2 School of Earth and Environment, University of Leeds, Leeds, LS2 9JT, UK
3 SINOPEC Star Petroleum Company, Beijing, 100094

Abstract: The simultaneous flow of gas and water is controlled by a threshold pressure gradient (TPG) effect during CO_2 injection of tight gas reservoirs for enhanced gas recovery (EGR) or CO_2 storage. The TPG effect is dynamic because it varies with both the effective stress and the water saturation. The sensitivity of TPG to effective stress and mobile water is affected by the pore-throat microstructure. In this paper we report the results of dynamic TPG tests on 6 cores with similar permeability. The influence of pore-throat microstructure on the sensitivity of the TPG to stress and to mobile water was also quantitatively studied using a fractal method, and the distribution of the threshold pressure and corresponding gas production loss were calculated during CO_2 injection in tight gas reservoirs. The test results show that TPG decreases logarithmically with the increase of pore fluid pressure during CO_2 injection, a change of 0.1-50 MPa in pore fluid pressure corresponding to 1.8-3.5 times increase of the TPG variation. The TPG increases exponentially by 3.5-6.7 times from irreducible water saturation to a mobile water saturation of 30%. The fractal dimension (D) of the heterogeneity of the rock pore-throat microstructure has a linear relationship with both stress sensitivity coefficient (λ) and mobile water sensitivity coefficient (η), with the larger values of λ and η being associated with more heterogeneous pore-throat microstructures. The reservoir threshold pressure showed a significant nonlinear distribution in near-well reservoirs at low bottom-hole flow pressures of the production well during CO_2 injection. The calculated gas well production loss due to a dynamic threshold pressure is 6-16% higher than that of fixed threshold pressure, and the difference is larger at low pressures. This research provides both theoretical and experimental data support for the design of CO_2 injection schemes in tight gas reservoirs and the establishment of accurate gas well production models.

Keywords: Tight gas reservoir, CO_2 injection, dynamic TPG, stress sensitivity, mobile water

sensitivity, gas production loss

Introduction

The development potential of tight gas reservoirs is considerable due to an extremely large proven hydrocarbon reserves [1]. Tight sandstone gas reservoirs typical exhibit poor physical properties and complex gas-water advection flow paths [2], which results in problems such as excessive attenuation of formation energy and gas production, and water breakthrough in gas wells in conventional development [3-4]. The CO_2 injection provides a new approach to enhanced gas recovery (EGR) in tight gas reservoirs, as well as being developed for use in long-term geological storage of CO_2 [5]. However, the pore-throat microstructure of tight gas reservoirs is complex, resulting in anfractuous pathways for gas flow that are also constrained by small pore-throat diameters. Consequently, the threshold pressure effect of gas-water two-phase transport in reservoirs is significant during CO_2 injection [6].

In tight gas reservoirs, the radius of the fluid flow channel is small, and the water films at narrow pore-throats generate a large flow resistance, even potentially forming a water slug to completely block the gas-water flow channel [7]. The gas needs to overcome the capillary resistance to break through the water slug, then the gas can start to flow through the pore-throat during CO_2 injection [8]. The threshold pressure effect appears during the gas-water transport in tight rock. When the pressure gradient as the driving force is less than the threshold pressure gradient (TPG) value, the water film or water slug is formed in the channels, blocking the gas flow path and stopping the gas moving. The smaller pore-throat size leads to a larger capillary resistance. Hence, the water distribution in the rock is mainly controlled by pore-throat microstructure, consequently, the rock pore-throat microstructure has a significant impact on the threshold pressure [9-10].

Significant variations of pore-throat microstructure and formation water distribution are caused by changes in effective stress and water saturation in tight rocks during CO_2 injection, resulting in variations of TPG. Consequently, the TPG is not fixed during the development of tight gas reservoirs. The TPG tests on cores indicate that TPG increases with the effective stress and water saturation, making it a dynamic effect [11-13]. The increase of effective stress results in the reduction of the size

of pore-throats, which increases the capillary resistance for gas and water to start flowing. The increase in water saturation causes more seepage paths to be blocked, which also increases the TPG in rocks.

The TPG stress sensitivity coefficient and the TPG mobile water sensitivity coefficient are defined in this work and have been used to describe the sensitivity characteristics of the dynamic TPG to the variation of rock effective stress and water saturation.

In addition, the results of TPG tests on cores also show that the TPG of tight rock is related to rock permeability [11]. A small rock permeability value usually indicates that the rock has a small pore-throat size and a complex pore-throat microstructure. The capillary resistance is large when the fluids begin to flow under the same conditions of pressure and water saturation, resulting in large TPG values in rocks with low permeability. The sensitivity of TPG to changes in water saturation is strong in rocks with low permeability, in particular, the influence of mobile water is much greater than that of irreducible water [6].

Previous TPG tests focus on the rock permeability as the influence factor. While, the permeability value is the macroscopic manifestation of the rock pore-throat microstructure, the rock pore-throat microstructure is the controlling factor for the water distribution in the pores. It os the pore-throat microstructure that has a direct control on the values and sensitivity of TPG to other parameters. Unfortunately, until now the effect of rock pore-throat microstructure on TPG values has not been studied quantitatively, and there is no report on the quantitative relationship between the sensitivity of TPG to changes in stress and mobile water saturation and the role that pore-throat microstructure in the process of CO_2 injection in tight gas reservoirs. In addition, both permeability and TPG stress sensitivities are attributed to variations in pore-throat microstructure caused by rock stress, but the differences in stress sensitivity between permeability and TPG have not previously been explored.

Furthermore, the results of previous studies were limited to cores and have not generalized to the distribution of threshold pressures in reservoirs. Indeed, the lack of relevant data of the dynamic TPG in the process of CO_2 injection has made it impossible to obtain an accurate threshold pressure distribution in the reservoirs [14-15]. There are problems in the process of CO_2 injection scheme design and gas production calculation. Specifically: ① The threshold pressure is related to reservoir pressure. The reservoir pressure decays to a certain value and then CO_2 injection is started, and the

optimal pressure of CO_2 injection for reducing the threshold pressure involves the selection of CO_2 injection timing and CO_2 injection parameters. ②The calculated threshold pressures by conventional methods increase linearly with distance by ignoring the effects of stress variation at different position in reservoirs. The selection of the optimal injection-production well spacing lacks a precise basis. ③ The threshold pressure in the conventional equation of gas production is a fixed value, which leads to a large deviation of the calculated gas production.

Consequently, the effect of factors such as pore fluid pressure and water saturation on the dynamic TPG need to be studied, and the effect of rock pore-throat microstructure on the TPG stress sensitivity and mobile water sensitivity need to be analyzed quantitatively. The relationship between the dynamic threshold pressure and the well spacing also needs to be calculated accurately. The difference in gas production loss due to dynamic/fixed TPG also needs to be compared. All these factors constitute the premise for the scientific development of CO_2 injection in tight gas reservoirs.

In this paper, the pore-throat microstructure heterogeneities of 6 cores with similar permeability were characterized quantitatively based on the test results of constant-rate mercury intrusion (CRMI) and fractal theory. The TPG values of CO_2 injection were tested at different pore fluid pressures and water saturations by an improved bubble method. New test equipment for accurately measuring the micro-pressure difference under high pressure was used and a monitoring system was built to accurately monitor the bubble movement in real time to improve the reliability and accuracy of TPG test results of the bubble method. The influence of the pore-throat microstructure on the TPG stress sensitivity coefficient and mobile water sensitivity coefficient was analyzed. The TPG stress sensitivity and the permeability stress sensitivity were compared. The dynamic threshold pressure distribution and the corresponding gas production loss in tight reservoir during CO_2 injection were calculated, and the difference between dynamic/fixed threshold pressure was studies. The influence of bottom-hole flow pressures in the production well on dynamic threshold pressure was also analyzed.

This research provides both theoretical and experimental data support for the design of CO_2 injection schemes in tight gas reservoirs and the establishment of accurate gas well production models.

Methodology

Materials

The cores used in the tests are taken from the tight gas reservoirs in the Ordos Basin, China. The depth of formation is 2910-3060 m, the formation temperature is 80±3.8°C. The porosity of rocks is 5.3-9.7%, and the permeability is 0.03-0.14×10^{-3} μm^2. Fifteen (15) matrix cores with similar permeability values were selected from 195 core samples in order to eliminate the interference of the difference in rock permeability on the experimental results. In this wat we were able to ascertain the nfluence of the difference in pore-throat microstructure on the dynamic TPG more accurately.

The selected cores were sampled and subjected to X-ray diffraction (D8 Focus X-ray diffractometer) and constant-rate mercury intrusion (CRMI; APSE-730 analyzer) tests to obtain information of rock mineral and pore-throat microstructure characteristics. Cores with similar mineralogy but large differences in the shape of the CRMI curve were selected (Figure 1, Table 1, Table 2). The cores were cut to 5.5 cm in length. The physical properties of the brine used in the tests are shown in Table 3. The CO_2 and CH_4 used in the tests have a high purity of 99.99% and were humidified.

Table 1. Basic parameters of the core samples.

Core number	Length cm	Diameter cm	Porosity %	Permeability 10^{-3} μm^2
H1	5.51	2.541	7.3	0.11
H2	5.56	2.532	6.8	0.10
H3	5.58	2.545	7.7	0.09
H4	5.54	2.534	7.9	0.11
H5	5.56	2.532	7.4	0.12
H6	5.53	2.537	7.2	0.10

Table 2. Types and contents of mineral in the cores.

Core number	Mineral type and content wt%					
	Quartz	K-feldspar	Plagioclase	Calcite	Dolomite	Clay
H1	48.4	12.5	29.2	1.3	1.7	6.9
H2	56.6	22.4	11.7	2.1	1.4	5.8
H3	47.4	28.6	9.2	6.3	1.8	6.7
H4	39.7	29.2	17.5	3.5	4.8	5.3
H5	44.7	15.2	29.2	2.2	2.2	6.5
H6	40.8	20.8	25.9	4.7	2.1	5.7

Table 3. Physicochemical and compositional properties of the reservoir water. measured at 20.0°C

Item	Value
Density (g/cm^3)	1.031
pH	6.74
K^+ (mg/L)	2318
Na^+ (mg/L)	1148
Ca^{2+} (mg/L)	4314
Mg^{2+} (mg/L)	390
Cl^- (mg/L)	22344
HCO_3^-(mg/L)	1148
SO_4^{2-}(mg/L)	1809
TDS (mg/L)	41614

TDS = Total dissolved solids

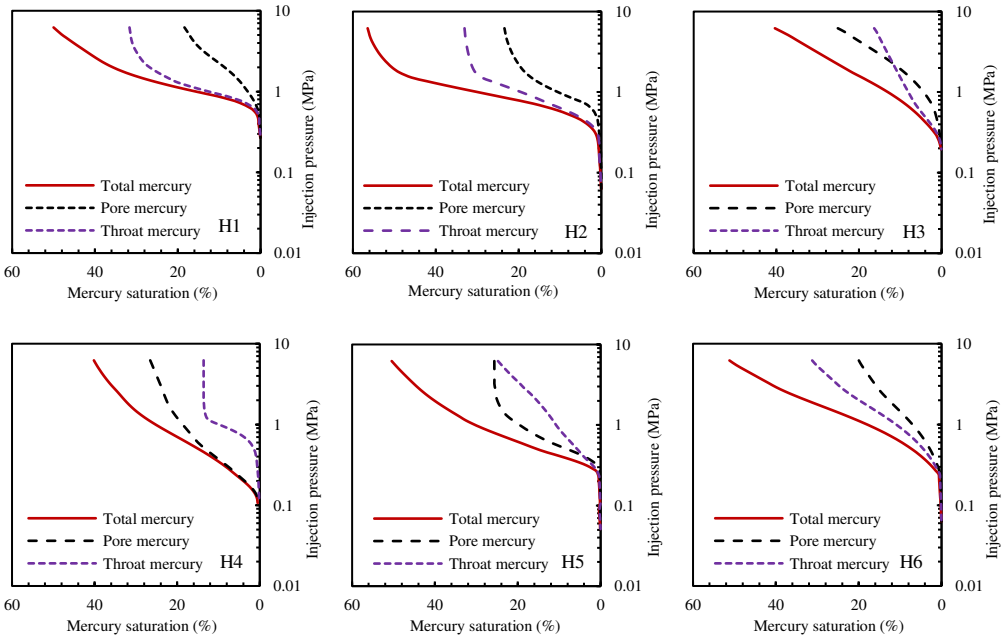

Figure 1. Core constant rate mercury intrusion curves for the total mercury, pore body mercury and pore-throat mercury for the 6 chosen core plugs.

Research methods

Quantitative characterization of rock pore-throat microstructure

, In this work fractal analysis and CRMI methods have been used to study the pore-throat microstructure because it was expected that the TPG is related to the rock pore-throat microstructure. The complexity and irregularity of the pore-throat microstructure can be characterized quantitatively by fractal dimension [16-17]. Consequently, in this work, the fractal theory approach is used to

quantitatively characterize the pore-throat microstructure based on the CRMI curves [18].

When the mercury as the non-wetting phase enters the pore-throat, the capillary resistance that needs to be overcome is given by,

$$P_c = \frac{2\sigma cos\theta}{r} \tag{1}$$

where P_c is the capillary pressure, MPa; σ is the interfacial tension, N/m; r is the pore-throat radius, m; θ is the wetting angle, °.

The rock pore-throat has fractal characteristics, the relationship between the capillary pressure and the wetting phase saturation is,

$$\log S = (D-3)\log P_c + (3-D)\log P_{min} \tag{2}$$

where S is the wetting phase saturation (%), D is the fractal dimension, dimensionless and (P_{min}), is the minimum capillary pressure (MPa).

The logarithm of wetting phase saturation (log(S)) and the logarithm of the capillary pressure (log(P_c)) have a linear relationship, when the rock pore-throat microstructure has fractal characteristics. The fractal dimension D of the pore-throat microstructure can be calculated according to the slope of the straight line. In fractal theory, the lower limit of D is 2, which represents regular pore shape or completely smooth pore surface; the upper limit of D is 3, which represents rough or completely irregular surface morphology of pore-throat [19]. The fractal dimension D increases with the complexity and heterogeneity of the rock pore-throat microstructure.

Threshold pressure test method

In this paper, we have measured the TPG when the gas in a core saturated with gas and water just begins to move. The bubble method is one of the common methods for experimental TPG tests on cores. Firstly, a small differential pressure is applied to the core for displacement, the outlet end of the core is immersed in water. The differential pressure is then increased to overcome the flow resistance. The gas in the core start to move, resulting in bubbles in water. At this point, the differential pressure on the core is the minimum threshold pressure [6], and hence the value of core TPG can be calculated.

In this paper, the bubble method for TPG test is improved. A thin pipette with bubbles was

connected to the outlet of the core. A camera and a computer were used to monitor the movement of the bubbles in real time. The monitoring of the gas flow is more accurate, resulting in a more precise threshold pressure. Moreover, the micro-pressure differential at high pressure is measured by the high-pressure dynamic differential pressure gauge, which can continuously monitor the variations of differential pressure on the order of 10^{-6} MPa at the system pressure of over 50 MPa.

Test equipment and process

Test conditions

The test conditions refer to the temperature and pressure of the reservoirs. The formation temperature was set to 80±0.5°C and the overburden pressure was 59±0.05 MPa. The TPG and gas permeability of cores were measured at different pore fluid pressures (0.1 to 50 MPa).

Tight gas reservoirs usually have high water saturation. Consequently, the threshold pressure tests were carried out for 4 different mean core water saturation values, which were set to the irreducible water saturation, and the moveable water saturations of approximately 10%, 20%, and 27%. The water saturations were monitored using nuclear magnetic resonance (NMR) measurement.

Test device and process

The main experimental device is the displacement system, which includes an high-precision displacement pump, tanks, pressure gauges, the micro-pressure difference measuring instrument, core holder, pipette, gas-liquid separator, gas flow meter, confining pressure pump, back pressure pump, back pressure valve, temperature control system, data acquisition system. A schematic diagram of the experimental device is shown in Figure 2.

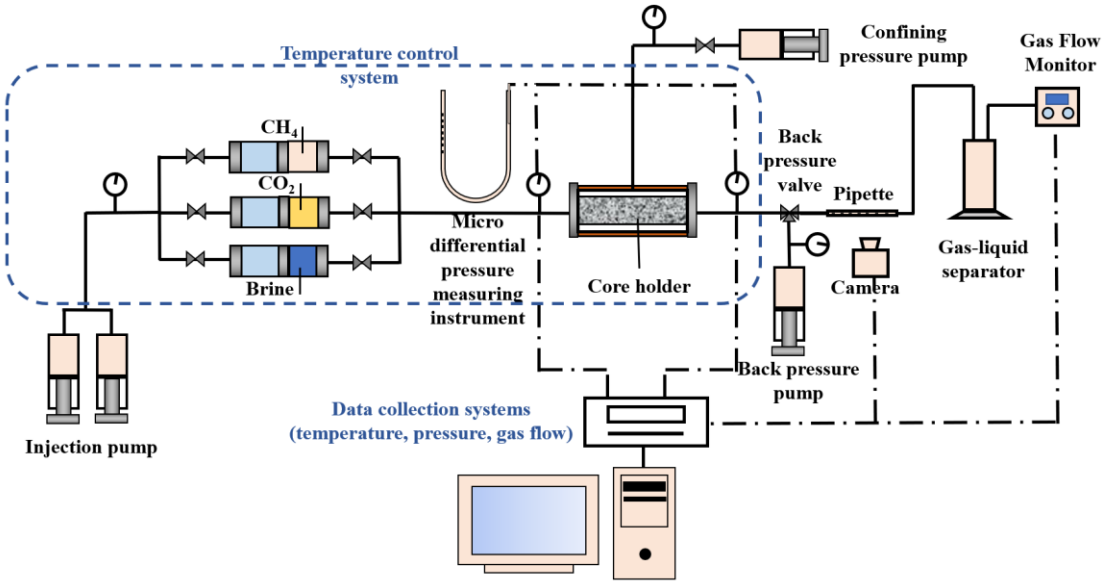

Figure 2. TPG test experimental device and process.

The experimental steps are as follows,

(1) **Device and fluid preheating**. The tanks were filled with brine, CO_2, CH_4. The tanks and the core holder were placed in the temperature controlled environment, and the temperature was set to 80±0.5°C for 24 hours.

(2) **Core water saturation setting**. The core was saturated with brine and placed in the core holder. The brine saturation was gradually decreased by CH_4 injection. The core holder was placed in the NMR equipment for NMR tests during CH_4 injection to obtain the brine distribution in the core. The CH_4 injection process stopped until the water saturation in the core reached a preset value.

(3) **The TPG tests** of CO_2 injection at different pore fluid pressure and irreducible brine saturation. The confining pressure was set to 59±0.05 MPa. The pressure at the outlet end of the core was stabilized at 0.1 MPa by the back pressure pump and back pressure valve, the differential pressure increased from 5×10^{-5} MPa by injecting CO_2 using the pump. The differential pressure was stabilized for 5 hours until the movement of bubbles was monitored. The pressure gradient was recorded at this point. Otherwise, the differential pressure was gradually increased until the gas started to flow. The TPG values and the core gas permeability were measured at 11 outlet pressures in the range of 0.1-50 MPa to obtain data as a function of effective pressure.

(4) **Repetitions for different water saturations**. The TPG values were tested by repeating steps (1)-(3) at different mobile water saturation at pore fluid pressure of 50 MPa.

(5) **Repetitions for different cores**. Steps (1)-(4) were repeated for different cores to complete the tests for all cores.

After each test, the core was measured by NMR to calculate the brine saturation. If the difference between the before test and after test brine saturation were less than 2%, the group of experimental data were considered to be reliable. Otherwise, the tests were repeated.

Results and discussion

Distribution of water and characterization of pore-throat microstructure of cores

Distribution of water in cores

The residual water saturation values in the pores with different sizes of the core during the CH_4 injection process are calculated according to the T_2 spectrum curve of NMR tests (definition: T_2=0.01-0.1 ms represents micropore, T_2=0.1-1 ms represents small pore, T_2=1-10 ms represents medium pore, T_2>10 ms represents macropore). The T_2 spectra of cores H2 and H5 are taken as examples and are shown in Figure 3. The water in the macropores is driven out in large quantities with the continuous CH_4 injection due to the smaller capillary resistance. The water saturation of small and medium pores also decreases, but to less of an extent. The water distribution in micropores is almost unchanged. The water in the macropores is almost completely driven out at the irreducible water saturation state.

The different water saturation values of the cores were calculated according to the T_2 spectrum curves, as shown in Table 4. The NMR test results of the rocks in the fully saturated water state represent the pore size distribution, but cannot reflect the pore-throat connectivity and cannot characterize the rock pore-throat microstructure [20].

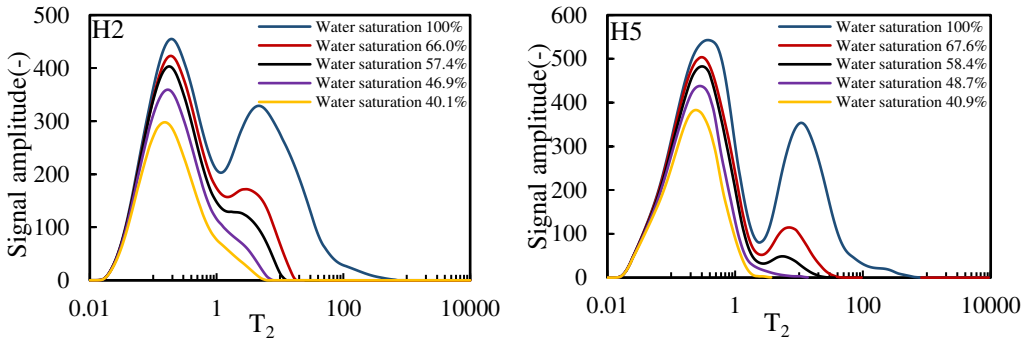

Figure 3. Changing NMR T_2 Spectra for two cores (H2 and H5) as they are progressively desaturated of water by CH_4.

Table 4. Water saturation of the core samples.

Core number	Water saturation %			
	S_{wc}	S_{w1}	S_{w2}	S_{w3}
H1	40.3	10.3	22.6	27.7
H2	41.1	7.8	18.3	27.5
H3	45.7	9.1	18.9	27.9
H4	49.8	13.5	19.1	26.3
H5	40.9	7.8	17.5	26.7
H6	45.6	12.5	20.7	28.6

Notes. S_{wc} is the irreducible water saturation. S_{w1}, S_{w2}, S_{w3} represent mobile water saturations.

Qualitative analysis of core pore-throat microstructure

The CRMI test results can characterize the pore-throat microstructure of the core samples. As shown in Figure 1, the total mercury injection curves of cores H1 and H2 are similar to the throat mercury injection curves ("S" type); the characteristics of total mercury injection are controlled by the throats. The total mercury injection saturations of core H1 and H2 increase steadily with injection pressure, a large amount of injected mercury corresponds to a narrow injection pressure range, and the core pores are well connected by throats, showing the characteristics of the homogeneous pore-throat microstructure [21].

The total mercury saturation and the injection pressure of the cores H3 and H4 show linear relationship with large slope, indicating that the connectivity among pores and throats with different sizes is poor, and the core pore-throat microstructure shows relatively strong heterogeneity. The total mercury injection saturation also has a linear relationship with the injection pressure in cores H5 and H6. The slopes of the linear relationship of cores H5 and H6 are smaller than that of core H3 and H4. The total mercury injection saturations of cores H5 and H6 are larger, with cores H5

and H6 showing relatively better pore-throat microstructure features than cores H3 and H4.

The results of the CRMI test show that, the cores exhibit differences in rock pore-throat microstructure and heterogeneity even if the permeability values of the rocks are similar. The heterogeneity of the pore-throat microstructure also has a great effect on the permeability and the fluid flow characters in rocks [22].

Quantitative analysis of rock pore-throat microstructure heterogeneity

The fractal analysis method has been used to characterize quantitatively the heterogeneity of rock pore-throat microstructure by providing a characteristic fractal dimension. As shown in Figure 4, The logarithm of wetting phase saturation (log(S)) and the logarithm of the capillary pressure (log (P_c)) exhibit a linear relationship. The log(S)-log(p_c) curve consists of two straight lines y_1 and y_2 with different slopes. The line y_1 corresponds to the large pore-throat (smaller log(p_c) corresponds to lower capillary pressure). The line y_2 corresponds to the small pore-throat (larger log(p_c) corresponds to higher capillary pressure) [23]. The fractal dimension D_1 of the large pore-throat and D_2 of the small pore-throat of the core were calculated based on Equation (2), as shown in Table 5.

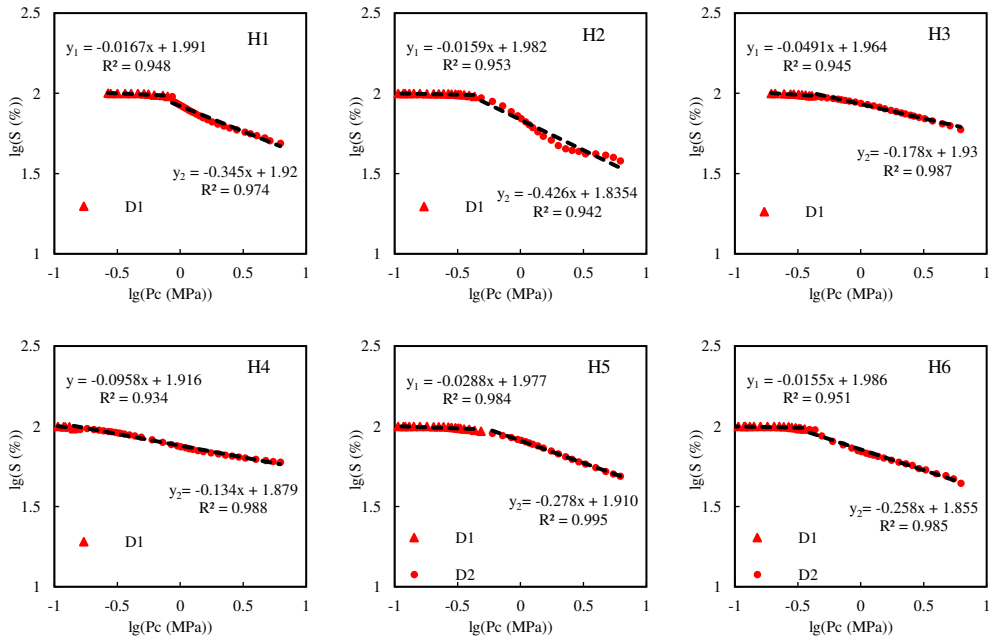

Figure 4. Logarithm of the water saturation as a function of the logarithm of the capillary pressure for all 6 core plugs (red symbols), together with best fit equations in log-log space for the low and high capillary pressure regimes.

Table 5. Fractal dimension of core pore-throat microstructure.

Core number		H1	H2	H3	H4	H5	H6
Fractal dimension	D_1	2.983	2.984	2.951	2.904	2.971	2.985
	D_2	2.655	2.574	2.822	2.866	2.722	2.742

The difference in D_1 values of cores is small, indicating that D_1 cannot effectively characterize differences in rock pore-throat microstructure. Furthermore, the D_1 values are close to 3, the fractal analysis method cannot effectively evaluate the microstructure of large pore-throat. The D_2 values of the small pore-throats range from 2.5 to 2.9, specifically, H2<H1<H5<H6<H3<H4. The large pores in the rock are mainly as space for storing fluid, and the narrow channels (small throats) that connect the pores are the key to control the fluid seepage characteristics in rocks. Consequently, the microstructure characteristics of small pore-throat are the main factors that determine the overall pore-throat microstructure characteristics of the rocks [24].

Moreover, when the rocks contain water in pores and throats, while the pores and throats are not fully saturated. Water, as the wetting phase, distributes itself preferentially in the fine pore-throats as water slugs and as water film on pore walls, while the gas phase is distributed in the centreof large pore-throats. The capillary force generated in the small pore-throats filled or partially filled with water provides the resistance of the gas-liquid two-phase flow during CO_2 injection [25]. It is this capillary force which results in the threshold effect of the CO_2 injection in tight gas reservoirs.

In this paper, we attempt to investigate the effect of rock pore-throat microstructure on the dynamic TPG. Consequently, it is reasonable to select the fractal dimension D_2 of small pore-throat to quantitatively characterize the heterogeneity of the core pore-throat microstructure. It is worth noting that the large fractal dimension of the rock pore-throat microstructure corresponds to larger irreducible water saturation values, indicating that the rock pore-throat microstructure is more complex, the water distribution in pore-throat is more complex [26] and more water is retained in the core at S_{wi}.

Dynamic TPG and pore fluid pressure

The measured TPG values during CO_2 injection at different pore fluid pressures are shown in Figure 5. The outlet of the core was open to the atmosphere (0.1 MPa) in the conventional threshold

pressure tests, and the variations of TPG with pore fluid pressure were not tested. However, the TPG values decreased by 45-85% as the pore fluid pressure increases from 0.1 MPa to 50 MPa), first rapidly, and then more gently, exhibiting the characteristics of dynamic variation

The TPG showed a logarithmic downward trend with pore fluid pressure,

$$\Delta P_{thresh} = \lambda \ln(p_p) + a \tag{3}$$

where ΔP_{thresh} is the TPG (MPa/m), p_p is the pore fluid pressure (MPa); a is the threshold pressure offset (MPa/m), and λ is the TPG coefficient (MPa/m).

The coefficient λ, which we define as the TPG Stress Sensitivity Coefficient, is a key parameter which controls the downward trend of the $\Delta P_{thresh}(p_p)$ curve. The λ coefficient describes the sensitivity of the TPG to changes in effective stress, and hence to changes in pore fluid pressure. A large value of $|\lambda|$ results in a large rate of change of TPG with the pore fluid pressure, i.e., a strong TPG stress sensitivity, as shown in Figure 5. The TPGs of cores H3 and H4 are most sensitive to changes in pore fluid pressure, while, the TPG stress sensitivity of cores H1 and H2 is relatively weak.

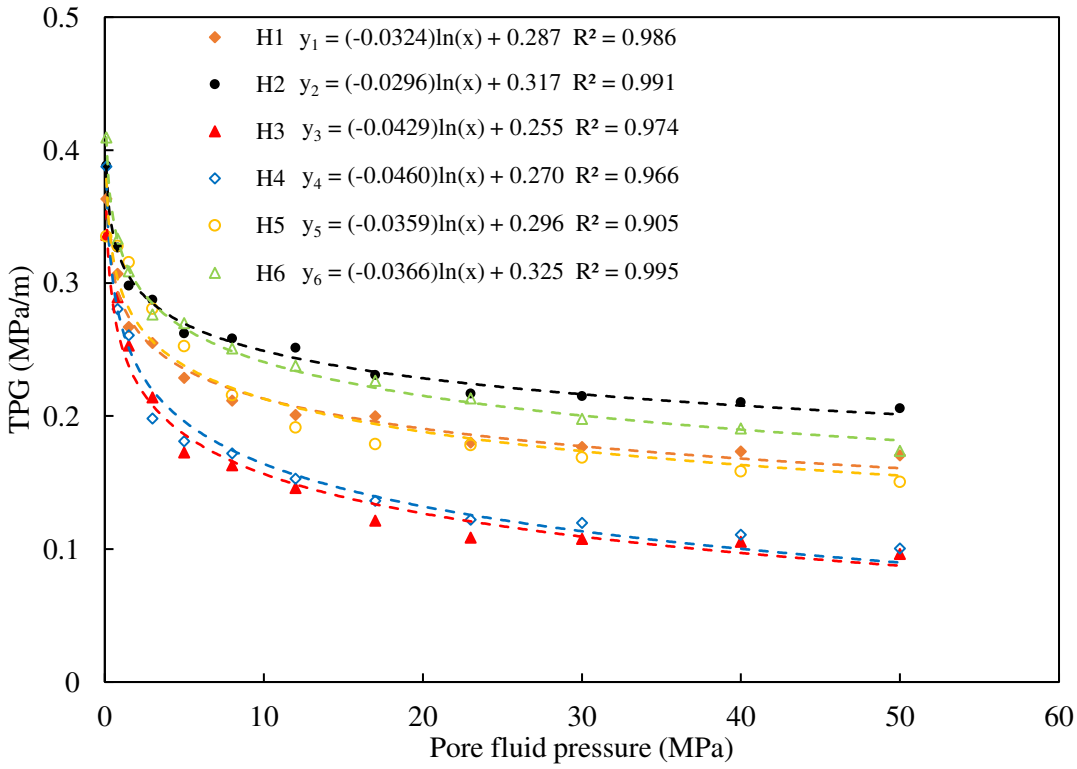

Figure 5. The TPG and pore fluid pressure of cores at irreducible water saturation.

The dynamic TPG of the two-phase fluid transport in tight gas reservoirs during CO_2 injection is attributed to the stress sensitivity of the pore-throat microstructure. The size of the pore-throat completely filled with water decreases as the effective stress increases, and the capillary resistance that CO_2 needs to overcome to drive the water becomes larger [12]. Moreover, the water films on the walls of some pores and throats merge with each other due to the reduced radius of pore-throats such that these pore-throats are filled with water and can be considered to be blocked by water slugs [27]. The development of water slugs makes the connectivity between the pores and throats worse, increasing further the threshold pressure (Figure 6a→6b).

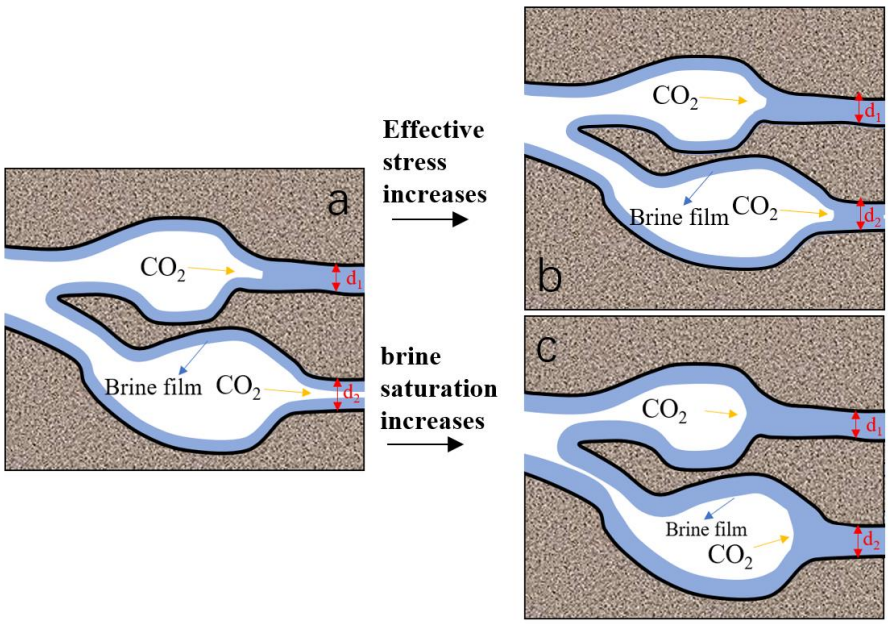

Figure 6. Schematic diagram of the TPG stress sensitivity and TPG mobile water saturation sensitivity mechanism. a→b Effect of effective stress variation on pore-throat shape and water distribution in pore-throat; a→c Effect of mobile water saturation variation on water distribution in pore-throat.

The TPG is controlled by the water distribution in the pore-throats. The wettability of the pore walls and the pore-throat microstructure determine the water distribution in the pore-throats [28]. The test results in Table 3 are from core samples which are all matrix sandstones, with little variation in mineralogy. The cores were immersed in water before the tests and the water was a strong wetting phase in the pore-throat of the cores. Consequently, in this paper, the difference in water distribution of the 6 cores is mainly controlled by the difference in complexity and heterogeneity of the pore-

throat microstructure, that is, the difference in TPG is mainly related to the fractal dimension of the pore-throat microstructure.

Figure 7 shows that the fractal dimension D of the rock pore-throat microstructure has a linear relationship with the TPG stress sensitivity coefficient λ. This suggests that the complexity of the pore-throat microstructure is a factor controlling the stress sensitivity of the TPG; a strong heterogeneity of the rock pore-throat microstructure results in a strong TPG stress sensitivity. Large fractal dimension values indicate a complex pore-throat microstructure, which will result in a more heterogeneous water distribution in the pore-throats [29]. Displacement in large pore throats only requires small pressures, but the smallest pore throats require very high pressures. For fluid flow to occur, both displacement process must operate together. Hence, flow is controlled by the small pre-throats and provide a high value of TPG.

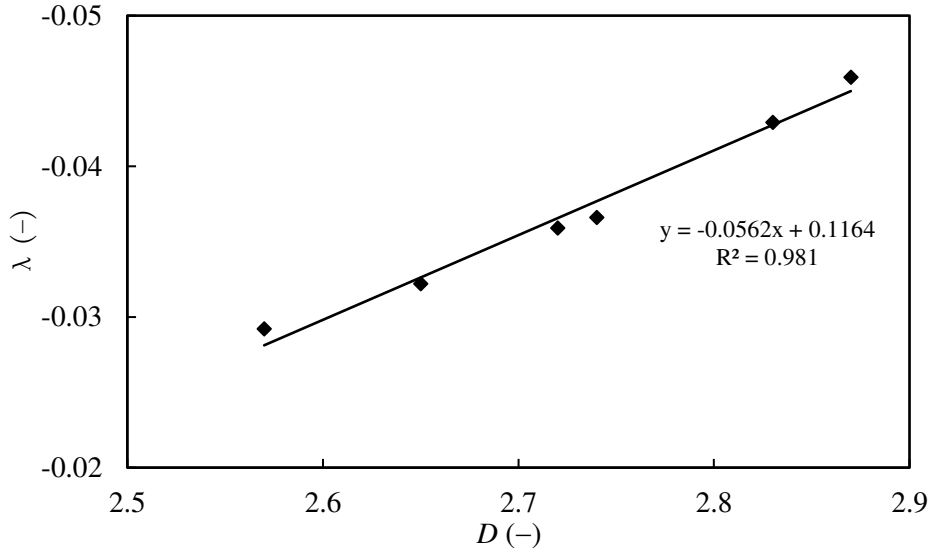

Figure 7. The heterogeneity of rock pore-throat microstructure (D) and stress sensitivity coefficient of the TPG (λ).

Stress sensitivity of TPG and permeability

Rocks with small permeability have previously been considered to exhibit strong TPG stress sensitivity [5], due to the same mechanism which causes the rock permeability's sensitivity to stress. The initial permeability values of the dry cores selected in this paper are almost the same, while the

permeability values are a macroscopic reflection of the ability of single-phase gaseous fluid to flow in dry cores with different pore-throat microstructures. The flow of two phases, such as a gas and a liquid, shows more complex characteristics in these cores [30]. Consequently, we can infer that differences in the ability of non-wetting fluids to displace water and move through water-wet cores must depends upon more factors than permeability alone.

In addition, variability in pore-throat microstructure can also lead to different stress sensitivities, irrespective of permeability or water saturation. Hence, the pore-throat microstructure is a common factor that controls both TPG stress sensitivity and permeability stress sensitivity.

The difference in the influence of pore-throat microstructure on the gas permeability stress sensitivity and the threshold pressure stress sensitivity has been analyzed at same initial permeability of dry cores, by excluding the influence of the difference in initial permeability. Figure 8 shows the relationship between gas permeability and pore fluid pressure at irreducible water saturation shows an exponential increase trend,

$$K_g = be^{\gamma p_p} \quad (4)$$

where K_g is gas permeability at irreducible water saturation ($\times 10^{-3}$ μm^2), p_p pore fluid pressure (MPa), and b and γ are dimensionless coefficients.

Figure 8 shows that gas permeability is related to pore fluid pressure, with permeability increasing with increasing pore fluid pressure. The rate of change of permeability increase is small at low applied pore fluid pressures (high effective pressures) and becomes greater at pore fluid pressure increases (effective pressure decreases). This contrasts markedly with the sensitivity of the TPG to increasing pore fluid pressure (Figure 6), where not only the TPG dereased with increasing pore fluid pressure, but the greatest rate of change in TPG occurred for small increases of pore fluid pressure (high effective pressures), with lower rates of change of TPG with pore pressure occurring at higher pore fluid pressures (lower effective pressures).

In addition, the overall sensitivity of the TPG to the pore fluid pressure variations is weaker than that of gas permeability. Unlike the TGP dependence of pore fluid pressure ($\Delta P_{thresh}(p_p)$)curves, which we have already seen follow a logarithmic relationship, the permeability dependence on pore fluid pressure ($K_g(p_p)$) curves show an exponential relationship. The TGP decreases to between 28% and 55% of its original value, while the permeability increases by 8-13 times for gas permeability,

both for a pore fluid pressure variation from 0.1 to 50 MPa

The parameter γ is the stress sensitivity coefficient of gas permeability at irreducible water saturation. The value of γ is in the range of 0.043-0.052 in this work, and also has a linear relationship with the fractal dimension D (Figure 9).

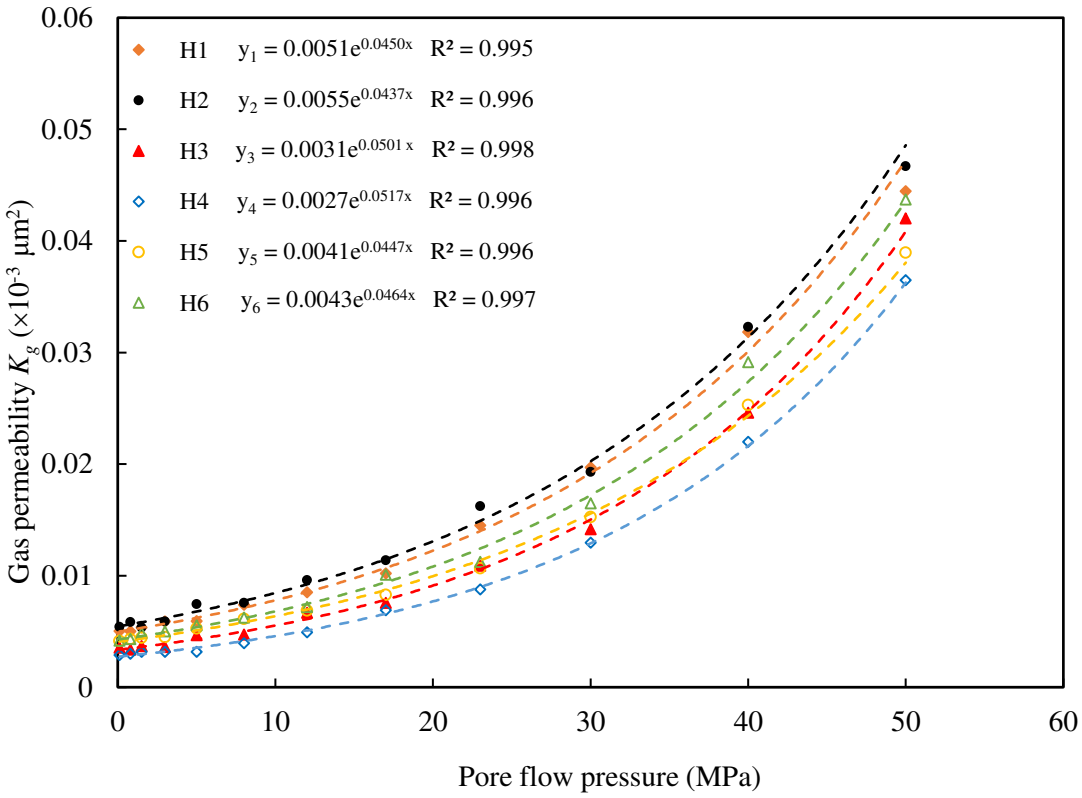

Figure 8. Gas permeability and pore fluid pressure of cores at irreducible water saturation.

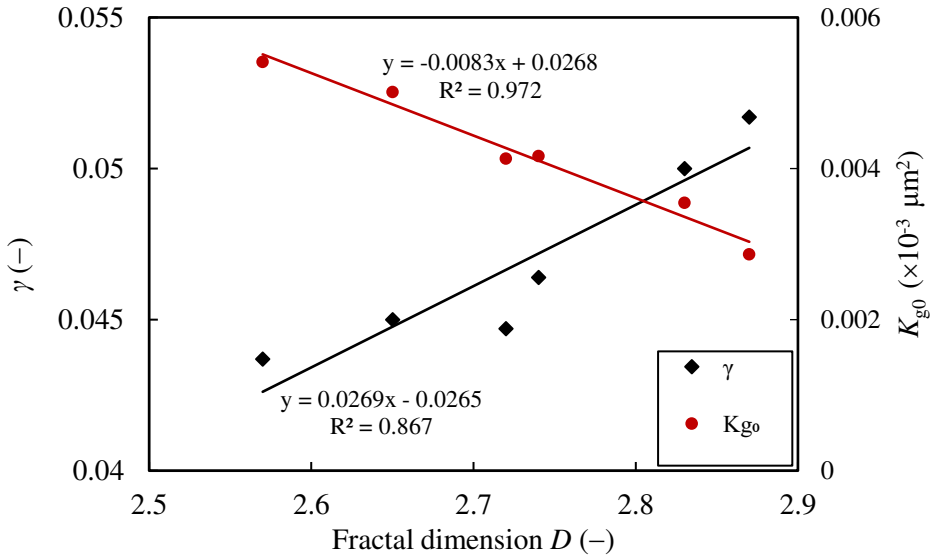

Figure 9. Core pore-throat microstructure (D), gas permeability stress sensitivity coefficient (γ) and gas permeability at pore fluid pressure of 50 MPa and at irreducible water saturation (K_{g0}).

There is a small difference in permeability values of the cores selected in tests, while the initial gas permeabilities K_{g0} (at pore fluid pressure of 50 MPa and at irreducible water saturation, the maximum value of K_g) of the rocks are quite different. As shown in Figure 9, K_{g0} has a linear negative correlation with the fractal dimension D of the rock pore-throat microstructure. Consequently, the apparent permeability (K_{g0}) of rocks with the same permeability (dry cores) at certain conditions is still controlled by the complexity of the rock pore-throat microstructure characteristics.

The large initial permeability value of the dry rocks is considered to results in the weak stress sensitivity of TPG and permeability [5-6,31]. However, Figure 10 shows that the large values of K_{g0} results in the small values of $|\lambda|$ and γ, that is, the TPG and permeability stress sensitivity are weak when K_{g0} is large. Furthermore, both the K_{g0}-$|\lambda|$ and K_{g0}-γ have linear relationships, respectively. Consequently, we come to the conclusion that the apparent initial permeability (in this case, K_{g0}, not the initial permeability of the dry core) is still strongly related to the stress sensitivity of TPG and permeability.

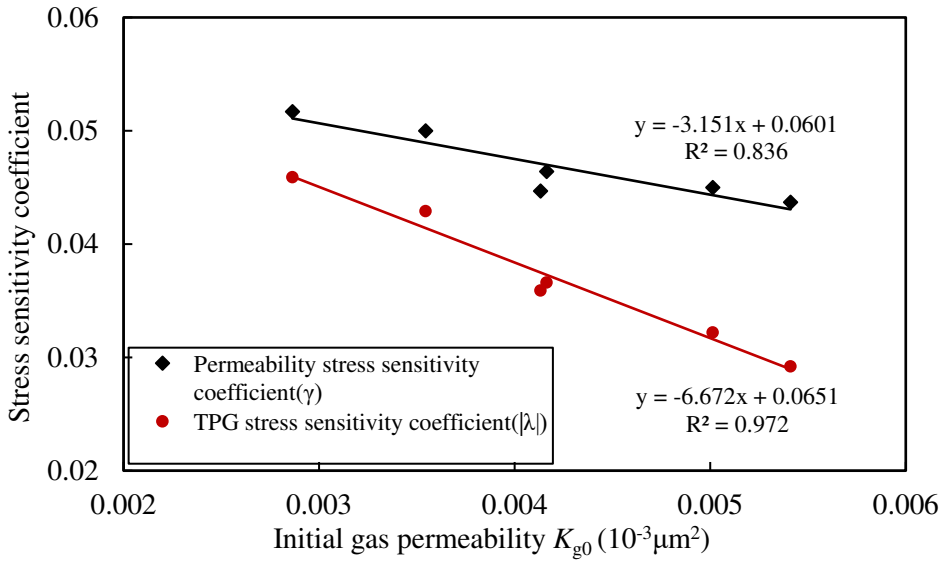

Figure 10. Initial gas permeability at irreducible water saturation versus stress sensitivity coefficients of permeability and TPG.

Dynamic TPG and water saturation

The variations of rock water saturation can directly lead to a significant variation of water distribution in pore-throats. This is especially the case when the water saturation is larger than the irreducible water saturation, where a large number of effective flow paths are blocked by water, such that the TPG increases rapidly [6]. Figure 11 shows the relationship between the TPG and the mobile water saturation at the pore fluid pressure of 50 MPa,

$$\Delta P_{thresh} = ce^{\eta S_{mob}} \quad (5)$$

where ΔP_{thresh} is the TPG (MPa/m), S_{mob} mobile water saturation (%), c is the TPG offset (MPa/m). The coefficient η (units of per %) is defined as the mobile water sensitivity [i.e., $S_{mob} = S_w$-S_{wi}] coefficient of the TPG.

Figure 11 shows that the increase of the $\Delta P_{thresh}(S)$ is relatively slow at the low mobile water saturations. The TPG is more sensitive to variations of water saturation at high water saturation. The initial value of TPG at S_{wi} (i.e., S_{mob}=0) varies in the range from 0.33 to 0.42 MPa/m, but increases exponentially as water saturation increases until it reaches 3.5-6.7 times its initial value by the time that S_{mob}=30%. The TPG is more sensitive to mobile water than to the pore fluid pressure.

This is because the irreducible water generally exists in the form of water film on the walls of

larger pores, or occupies the small pore-throats, and it is difficult for this type of water to flow [32]. A small proportion of mobile water can block the pores that are not occupied by irreducible water due to the free-flowing nature of mobile water. The gas flow is greatly affected by the mobile water (see the process illustrated in Figure 6a→c). When the mobile water saturation increases to a certain level, some large pore-throats are also filled with water. The flow paths with large size and small flow resistance are blocked, resulting in a part of large flow channels becoming blocked where they had previously been patent to gas. The total length of flow paths blocked by water slug is longer, resulting in a more significant flow threshold effect [29]. Moreover, the dynamic effect of TPG caused by this direct water distribution variation (the increase of mobile water saturation) is much more significant than the indirect effect of the pore-throat size variation caused by stress sensitivity. Consequently, the TPG is more sensitive to mobile water than the pore fluid pressure.

When the water saturation of cores with different pore-throat microstructures increases by the same value, the distributions of the increased mobile water are different in different cores, which in turn affects the sensitivity of TPG to mobile water. Figure 12 shows the mobile water sensitivity coefficient η of TPG also has a linear relationship with the fractal dimension D. The slope of the $\eta(D)$ fitting line is larger (0.796) than that of $\lambda(D)$, indicating that the TPG mobile water sensitivity coefficient η is relatively more sensitive to the heterogeneity of the pore-throat microstructure.

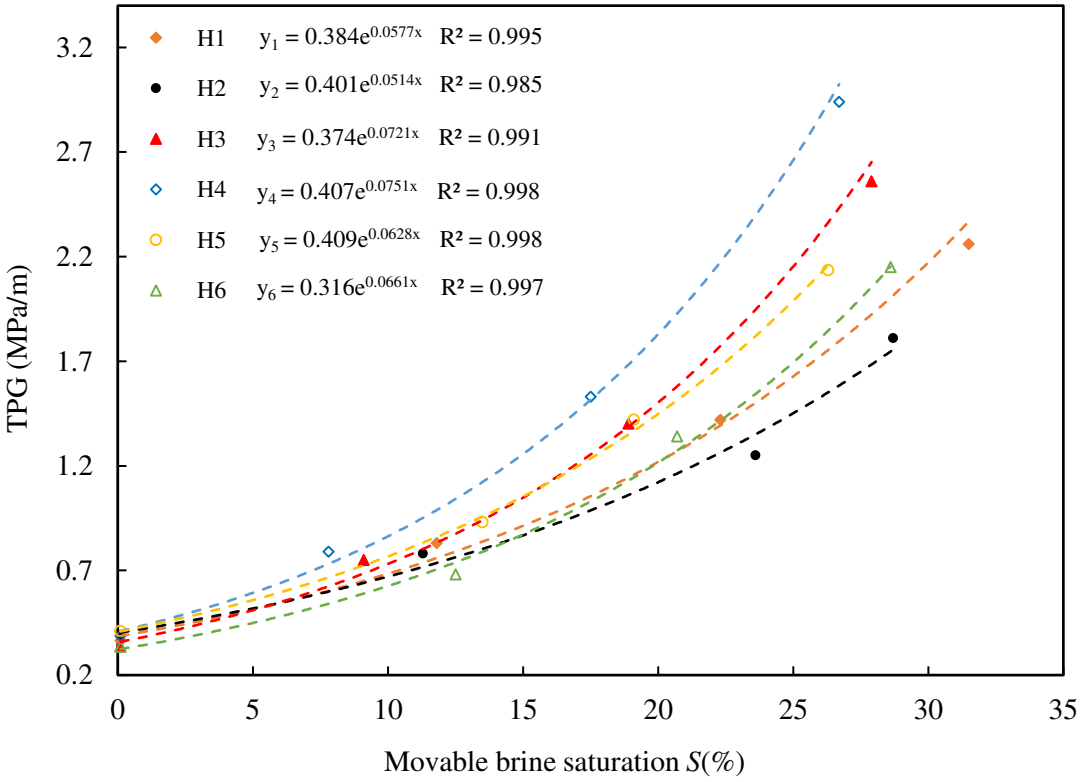

Figure 11. TPG of cores at different mobile water saturations.

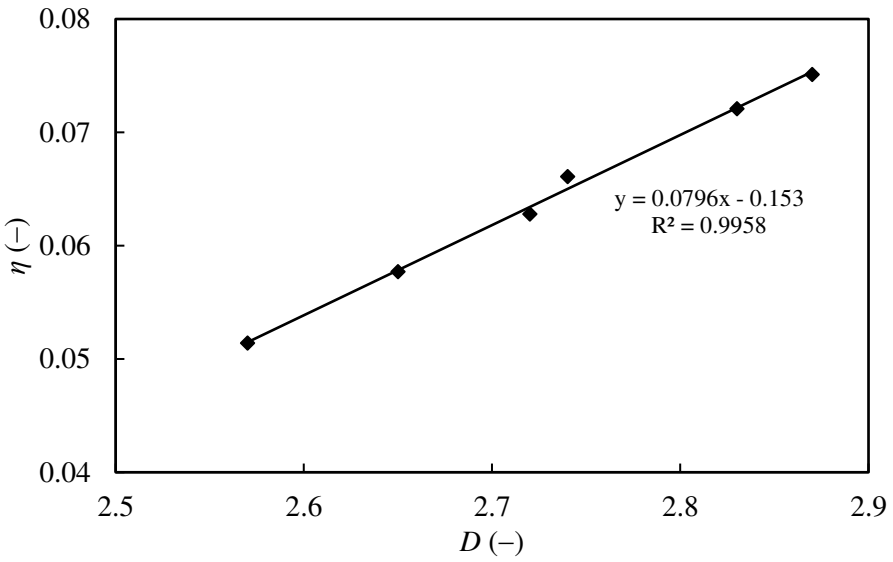

Figure 12. Heterogeneity of core pore-throat microstructure (D) and sensitivity coefficient to mobile water saturation (η).

Threshold pressure distribution and gas production loss

Once the pressure of tight gas reservoir decays to a certain value, CO_2 injection is implemented. When the differential pressure between the injection well and the production well is larger than the threshold pressure, that is, the differential pressure gradient at any position in the reservoir is greater than or equal to the TPG, then the fluid starts to flow [33-34]. This condition may be expressed as,

$$\begin{cases} v = 0 & \dfrac{dp}{dl} \le \Delta P_{thresh} \\ v = \dfrac{K_g}{\mu}\left(\dfrac{dp}{dl} - \Delta P_{thresh}\right) & \dfrac{dp}{dl} > \Delta P_{thresh} \end{cases} \tag{6}$$

where v is the gas flow rate (m/s), dp/dl is the differential pressure gradient (MPa/m), ΔP_{thresh} is the TPG (MPa/m), K_g is the gas permeability ($\times 10^{-3}$ μm^2), and μ is the gas viscosity (mPa·s).

When the TPG is considered to not vary with the effective stress, the threshold pressure distribution of the reservoir increases linearly along the axis of the injection and production wells during CO_2 injection [35]. However, the TPG changes with the variation of pore fluid pressure according to the experimental results in this paper. The pore fluid pressure is related to CO_2 injection pressure (displacement pressure), and the displacement pressure and the threshold pressure interact with each other. That is, when the injection pressure is continuously increased to overcome the threshold pressure, the threshold pressure decreases instead due to the increased reservoir pressure. The two factors are coupled with each other to change dynamically. Finally, the differential pressure gradient of displacement is equal to the TPG. At this point, this threshold pressure is the maximum in the reservoir and gas-liquid flow begins. This injection pressure is also the minimum effective CO_2 injection pressure. The distribution of the threshold pressure along a radial distance from injection well to production well is difficult to predict by simple linear calculation. Consequently, a calculation method of dynamic threshold pressure distribution in reservoir has been established in this paper and the results are given below.

The reservoir is assumed to be homogeneous in permeability for the purposes of the calculation process. The parameters such as reservoir permeability, and pore-throat microstructure heterogeneity and TPG stress sensitivity at irreducible water saturation are taken as the average values of the 6 cores. The values of the coefficients λ and a in Equation (3) are also taken as the

average values of the 6 cores respectively. Hence,

$$\Delta P_{thresh} = -0.0371 \ln(p_p) + 0.291 \tag{7}$$

According to Equation (6), when v=0,

$$\frac{dp_p}{dl} = -0.0371 \ln(p_p) + 0.291 \tag{8}$$

Equation (8) can be solved by the ordinary differential equation solver 'ode45' function in MATLAB to obtain the numerical solution. The production well is the calculation starting point, the CO_2 injection end is the calculation end point. Three sets of initial values are given as (i) l=0 m (the position of production well, l is the distance from the production well), p_p=0.1 MPa (the bottom-hole flowing pressure of production well when CO_2 starts to be injected into the reservoir), (ii) l=0 m, p_p=5 MPa, and (iii) l=0 m, p_p= 15 MPa. These calculated dynamic TPG results are shown compared with the results of calculations using a conventional fixed TPG with the same parameters inFigure 13. The effect of effective stress on TPG is not considered in the conventional threshold pressure tests, and the effective stress of the rock set during TPG tests is small. Consequently, the fixed TPG is taken as the average value of the TPG of the 6 cores at pore fluid pressure of 50 MPa.

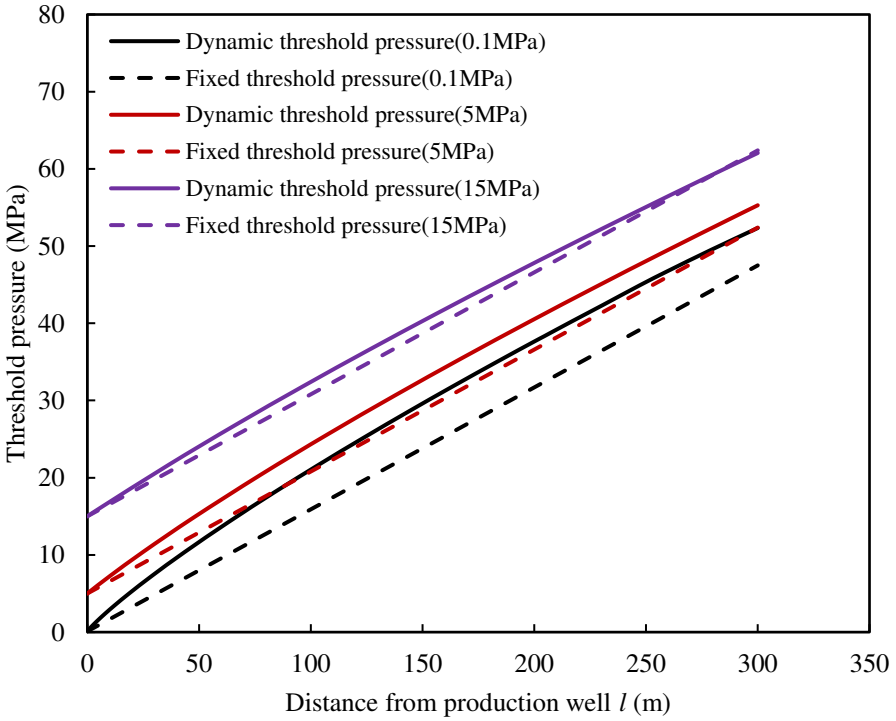

Figure 13. Threshold pressure distribution in reservoir when CO_2 starts to be injected.

As expected, the distribution of threshold pressure along distance in reservoir is not linear when

CO_2 is injected to displace gas. The threshold pressure increases more rapidly near the production well, while it increases at a smaller rate and approximately linearly when l >100 m. This is because the pore fluid pressure of rocks at a large distance from the production well (closer to the injection end) is large during the CO_2 injection for increasing reservoir pressure, the TPG stress sensitivity is weak, and the TPG variation is small, so the TPG can be approximated as a fixed value.

By contrast, close to the production well the TPG variation is larger, resulting in a non-linear distribution of threshold pressure. In addition, the lower initial bottom-hole flowing pressure of production well results in the more significant nonlinear distribution of the threshold pressure in reservoirs. It shows that the threshold pressure in the reservoir during CO_2 injection changes more at lower reservoir pressure.

Furthermore, the dynamic threshold pressure of the reservoir is greater than the fixed threshold pressure. As shown in Figure 14, the difference (ΔTPG) between the dynamic/fixed threshold pressure first increases and then decreases with the distance. This indicates that the dynamic effect of TPG is not significant at high reservoir pressure (close to the injection end), but the difference between dynamic TPG and fixed TPG is large and significant at the low reservoir pressures close to the production end. The dynamic threshold pressure distribution curve is close to a straight line at high bottom-hole flow pressure in the production well, and the overall ΔTGP is small. The distance is small when ΔTGP reaches the maximum value at high bottom-hole flow pressure in the production well, showing that the well spacing has relatively little effect on ΔTGP.

In summary, when the stress sensitive effect of the TPG is ignored during the CO_2 injection process, the threshold pressure is smaller than the actual value. The large well spacing corresponds the large calculated threshold pressure deviation. When the bottom-hole flow pressure of the production well is high, the calculated threshold pressure deviation is small. However, the dynamic threshold pressure effects cannot be ignored at low reservoir pressures.

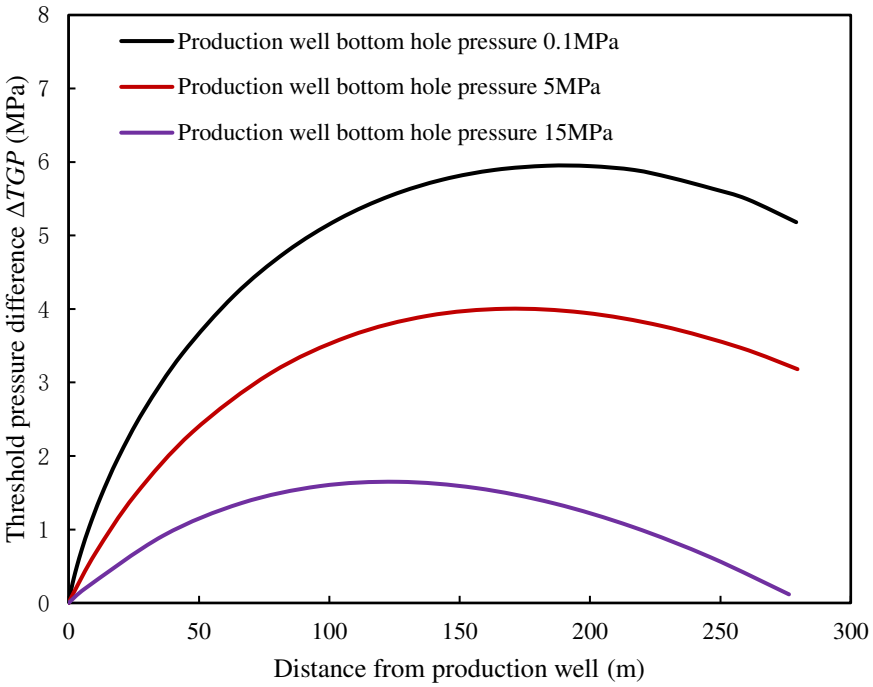

Figure 14. The distribution of the difference between the dynamic/fixed threshold pressure in reservoir.

The TPG results in the loss of displacement pressure for gas production in tight gas reservoirs, which is ultimately manifested as the loss of gas well production. According to the results in Figures 13 and 14, it can be expected that the gas production loss caused by the fixed TPG is clearly different from that of the dynamic threshold pressure at the same reservoir conditions. Generally, the fixed threshold pressure is smaller than the dynamic threshold pressure, and the calculated gas production of the fixed threshold pressure is greater than that of dynamic threshold pressure.

According to Equation (6), the plane radial flow in a homogeneous, horizontal, and equal-thickness reservoir can be obtained as[36],

$$\begin{cases} q_0 = \dfrac{2\pi r h K_g}{\mu}\dfrac{dp_p}{dr} \text{ (Without TPG)} \\ q_1 = \dfrac{2\pi r h K_g}{\mu}\left(\dfrac{dp_p}{dr} - \Delta P_{thresh}\right) \text{ (Fixed TPG)} \\ q_2 = \dfrac{2\pi r h K_g}{\mu}\left(\dfrac{dp_p}{dr} - \Delta P_{thresh}(p_p)\right) \text{ (Dynamic TPG)} \end{cases} \tag{9}$$

where K_g is the gas permeability ($\times 10^{-3}$ μm^2), μ is the gas viscosity (mPa·s), p_p is the pore fluid

pressure (MPa), r is the distance from production well (m), the three parameters q_0, q_1, and q_2 are the flows at r (m^3/s), and h is the effective thickness of the layer (m). The gas production loss (L_p, %) due to the dynamic/fixed TPG of the production well can be obtained from,

$$L_p = (100 - \frac{Q}{Q_0} \times 100) \tag{10}$$

where Q is gas well production with (dynamic/fixed) threshold pressure (m^3/d), and Q_0 is gas well production without threshold pressure (m^3/d). Assuming the original formation pressure p_e=50 MPa in tight gas reservoir, supply radius r_e=100 m, wellbore radius r_w =0.1 m, L_p was calculated through MATLAB, and is shown in Figure 15.

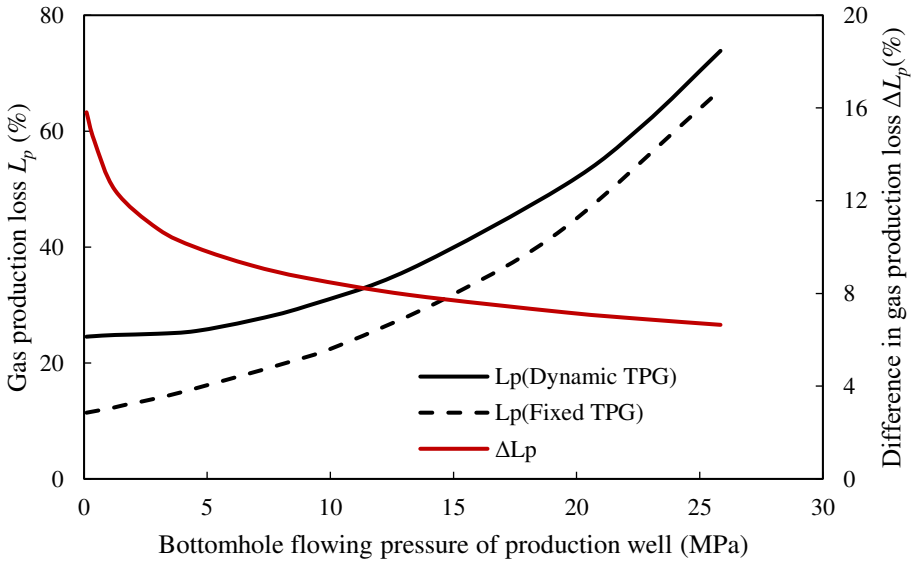

Figure 15. Gas production loss at the dynamic/fixed threshold pressure.

Figure 15 shows that the L_p increases with the bottom-hole flowing pressure. This is because a large bottom-hole flowing pressure implies a small displacement differential pressure. The threshold pressure as the loss of displacement differential pressure accounts for a large proportion of the displacement differential pressure resulting in a large L_p and a low production efficiency. The L_p is over 60% at bottom-hole flowing pressure of 25 MPa. The L_p is also over 10% at the minimum bottom-hole flowing pressure of 0.1 MPa (the maximum displacement differential pressure of 50 MPa). It is worth noting that although the decrease of bottom-hole flowing pressure can reduce L_p at low pressures, it can increase the TPG values and the sensitivity of TPG to pressure changes (increasing L_p). Consequently, the L_p increases slowly at lower bottom-hole flowing pressures. In

particular, the L_p of dynamic threshold pressure is 6-16% higher than that of fixed threshold pressure. Moreover, the difference in production loss (ΔL_p) between the dynamic and fixed threshold pressures decreases with the bottom-hole flow pressure. The ΔL_p is over 15% at a low bottom-hole flowing pressure, which is significant and cannot be ignored. It is worth noting that the ΔL_p decreases rapidly at low bottom-hole flowing pressures, the ΔL_p is more sensitive to pressure variations at low pressures. This is because the dynamic TPG is sensitive to pressure changes at lower pressures, and the difference between the fixed TPG and the dynamic TPG is large.

Conclusions

The dynamic threshold pressure gradient (TPG) and gas permeability of tight cores with similar permeability were measured experimentally using an improved bubble method. Measurements were made as a function of pore fluid pressures and water saturations during CO_2 injection.

The influence of pore-throat microstructure on the TPG stress sensitivity, permeability stress sensitivity, and mobile water sensitivity has been analyzed quantitatively using a method based on fractal theory. The distribution of the dynamic/fixed threshold pressure and the gas production loss in tight gas reservoir during CO_2 injection were calculated at different bottomhole flowing pressure.

We arrived at the following conclusions.

(1) The TPG values of tight gas reservoir rock with permeability of 0.1×10^{-3} μm^2 during CO_2 injection are 0.09-0.41 MPa/m, and the TPG shows a logarithmic downward trend with the increase of pore fluid pressure. The TGP decreases to between 28% and 55% of its original value as the pore fluid pressure was varied from 0.1 to 50 MPa.

(2) The TPG exponentially increases with mobile water saturations, and the TPG values are 0.33-2.94 MPa/m at the flow fluid pressure of 50 MPa. The TPG increases by 3.5-6.7 times from irreducible water saturation to the mobile water saturation of 30%.

(3) The TPG stress sensitivity coefficient λ and TPG mobile water sensitivity coefficient η have linear relationships with the fractal dimension D of the rock pore-throat microstructure. The strong heterogeneity of the pore-throat microstructure results in the strong TPG sensitivity. The sensitivity of the TPG to the variation of pore fluid pressure is weaker than that of the gas permeability. The rock TPG is more sensitive to the mobile water than the stress change.

(4) The nonlinear distribution of dynamic threshold pressure is significant during CO_2 injection at low reservoir pressure. The gas production loss of dynamic threshold pressure is 6-16% higher than that of fixed threshold pressure.

Acknowledgments

This research is supported by National Natural Science Foundation of China, "The formation mechanism of residual gas and liquid in coal seam and the geological constraints for effective production" (41872171), and "Cross-scale precipitation mode of asphaltene in ultra-deep sandstone reservoir during CO_2 flooding" (52104048).

References

[1] Zhang, T., Zhang, L., Wang, Y., Qiao, X., Feng, D., Zhao, W., & Li, X. (2020). An integrated well-pattern optimization strategy to unlock continental tight gas reservoir in China. *Energy*, *209*, 118449.

[2] Liu, G., Xie, S., Tian, W., Wang, J., Li, S., Wang, Y., & Yang, D. (2022). Effect of pore-throat microstructure on gas-water seepage behaviour in a tight sandstone gas reservoir. *Fuel*, *310*, 121901.

[3] Kulga, B., Artun, E., & Ertekin, T. (2018). Characterization of tight-gas sand reservoirs from horizontal-well performance data using an inverse neural network. *Journal of Natural Gas Science and Engineering*, *59*, 35-46.

[4] Gu, D., Ding, D., Gao, Z., Tian, L., Liu, L., & Xiao, C. (2019). A fractally fractional diffusion model of composite dual-porosity for multiple fractured horizontal wells with stimulated reservoir volume in tight gas reservoirs. *Journal of Petroleum Science and Engineering*, *173*, 53-68.

[5] Ding, J., Yan, C., He, Y., & Wang, C. (2021). Supercritical CO_2 sequestration and enhanced gas recovery in tight gas reservoirs: Feasibility and factors that influence efficiency. *International Journal of Greenhouse Gas Control*, 105, 103234.

[6] Tian W, Li A, Ren X, et al. The threshold pressure gradient effect in the tight sandstone gas reservoirs with high water saturation[J]. Fuel, 2018, 226: 221-229.

[7] Han, G., Liu, Y., Nawnit, K., & Zhou, Y. (2018). Discussion on seepage governing equations for low permeability reservoirs with a threshold pressure gradient. *Advances in Geo-Energy Research*, *2*(3), 245-259.

[8] Liu, W., Wu, Z., Li, J., Zheng, J., & Li, Y. (2020). The seepage characteristics of methane hydrate-bearing clayey sediments under various pressure gradients. *Energy*, *191*, 116507.

[9] Rudyk, Svetlana, and Amal Al-Lamki. (2015). Saturation-Height Model of Omani deep tight gas reservoir. *Journal of Natural Gas Science and Engineering*, 27: 1821-1833.

[10] Song, H., Cao, Y., Yu, M., Wang, Y., Killough, J. E., & Leung, J. (2015). Impact of permeability heterogeneity on production characteristics in water-bearing tight gas reservoirs with threshold pressure gradient. *Journal of Natural Gas Science and Engineering*, 22, 172-181.

[11] Ding, J., Yang, S., Nie, X., & Wang, Z. (2014). Dynamic threshold pressure gradient in tight

gas reservoir. *Journal of Natural Gas Science and Engineering*, *20*, 155-160.
[12] Ding, J., Yang, S., Cao, T., & Wu, J. (2018). Dynamic threshold pressure gradient in tight gas reservoir and its influence on well production. *Arabian Journal of Geosciences*, *11*(24), 1-6.
[13] Zafar, A., Su, Y. L., Li, L., Fu, J. G., Mehmood, A., Ouyang, W. P., & Zhang, M. (2020). Tight gas production model considering TPG as a function of pore pressure, permeability and water saturation. *Petroleum Science*, *17*(5), 1356-1369.
[14] Yin, S., Han, C., Wu, Z., & Li, Q. (2019). Developmental characteristics, influencing factors and prediction of fractures for a tight gas sandstone in a gentle structural area of the Ordos Basin, China. *Journal of Natural Gas Science and Engineering*, *72*, 103032.
[15] Zhang, Y., Jiang, S., He, Z., Wang, Y., Guo, M., Zhu, G., ... & Chen, G. (2022). Characteristics of heterogeneous diagenesis and modification to physical properties of Upper Paleozoic tight gas reservoir in eastern Ordos Basin. *Journal of Petroleum Science and Engineering*, *208*, 109243.
[16] Li, P., Zheng, M., Bi, H., Wu, S., & Wang, X. (2017). Pore throat microstructure and fractal characteristics of tight oil sandstone: a case study in the Ordos Basin, China. *Journal of Petroleum Science and Engineering*, *149*, 665-674.
[17] Qu, Y., Sun, W., Tao, R., Luo, B., Chen, L., & Ren, D. (2020). Pore–throat microstructure and fractal characteristics of tight sandstones in Yanchang Formation, Ordos Basin. *Marine and Petroleum Geology*, *120*, 104573.
[18] Zhang, F., Jiang, Z., Sun, W., Zhang, X., Zhu, L., Li, X., & Zhao, W. (2020). Effect of microscopic pore-throat heterogeneity on gas-phase percolation capacity of tight sandstone reservoirs. *Energy & Fuels*, *34*(10), 12399-12416.
[19] Wu, Y., Liu, C., Ouyang, S., Luo, B., Zhao, D., Sun, W., ... & Zang, Q. (2022). Investigation of pore-throat microstructure and fractal characteristics of tight sandstones using HPMI, CRMI, and NMR methods: A case study of the lower Shihezi Formation in the Sulige area, Ordos Basin. *Journal of Petroleum Science and Engineering*, *210*, 110053.
[20] Wang, L., Zhao, N., Sima, L., Meng, F., & Guo, Y. (2018). Pore microstructure characterization of the tight reservoir: systematic integration of mercury injection and nuclear magnetic resonance. *Energy & Fuels*, *32*(7), 7471-7484.
[21] Wang, J., Wu, S., Li, Q., Zhang, J., & Guo, Q. (2020). Characterization of the pore-throat size of tight oil reservoirs and its control on reservoir physical properties: A case study of the Triassic tight sandstone of the sediment gravity flow in the Ordos Basin, China. *Journal of Petroleum Science and Engineering*, *186*, 106701.
[22] Fan, N., Wang, J., Deng, C., Fan, Y., Wang, T., & Guo, X. (2020). Quantitative characterization of coal micromicrostructure and visualization seepage of macropores using CT-based 3D reconstruction. *Journal of Natural Gas Science and Engineering*, *81*, 103384.
[23] Wang, X., Pan, J., Wang, K., Ge, T., Wei, J., & Wu, W. (2020). Characterizing the shape, size, and distribution heterogeneity of pore-fractures in high rank coal based on X-ray CT image analysis and mercury intrusion porosimetry. *Fuel*, *282*, 118754.
[24] Guan, M., Liu, X., Jin, Z., & Lai, J. (2020). The heterogeneity of pore microstructure in lacustrine shales: Insights from multifractal analysis using N2 adsorption and mercury intrusion. *Marine and Petroleum Geology*, *114*, 104150.
[25] Wang, X., & Sheng, J. J. (2019). Multi-scaled pore network modeling of gas-water flow in shale formations. *Journal of Petroleum Science and Engineering*, *177*, 899-908.
[26] Huang, H., Sun, W., Ji, W., Zhang, R., Du, K., Zhang, S., ... & Zhang, X. (2018). Effects of

pore-throat microstructure on gas permeability in the tight sandstone reservoirs of the Upper Triassic Yanchang formation in the Western Ordos Basin, China. *Journal of Petroleum Science and Engineering*, *162*, 602-616.
[27] Liu, G., Wang, Y., Yin, H., Ding, Y., Lan, Y., & Yang, D. (2022). Determination of gas-water seepage characteristics with consideration of dynamic pore-throat microstructure in a tight sandstone gas formation. *Marine and Petroleum Geology*, *136*, 105440.
[28] Liu, B., Yang, Y., Li, J., Chi, Y., Li, J., & Fu, X. (2020). Stress sensitivity of tight reservoirs and its effect on oil saturation: A case study of Lower Cretaceous tight clastic reservoirs in the Hailar Basin, Northeast China. *Journal of Petroleum Science and Engineering*, *184*, 106484.
[29] Wang, Q., Yang, S., Glover, P. W., Lorinczi, P., Qian, K., & Wang, L. (2020). Effect of pore-throat micromicrostructures on formation damage during miscible CO2 flooding of tight sandstone reservoirs. *Energy & Fuels*, *34*(4), 4338-4352.
[30] Gao, H., Wang, C., Cao, J., He, M., & Dou, L. (2019). Quantitative study on the stress sensitivity of pores in tight sandstone reservoirs of Ordos basin using NMR technique. *Journal of Petroleum Science and Engineering*, *172*, 401-410.
[31] Hao, F., Cheng, L. S., Hassan, O., Hou, J., Liu, C. Z., & Feng, J. D. (2008). Threshold pressure gradient in ultra-low permeability reservoirs. *Petroleum Science and Technology*, *26*(9), 1024-1035.
[32] Lai, F., Li, Z., Zhang, W., Dong, H., Kong, F., & Jiang, Z. (2018). Investigation of pore characteristics and irreducible water saturation of tight reservoir using experimental and theoretical methods. *Energy & Fuels*, *32*(3), 3368-3379.
[33] Song, H., Liu, Q., Yang, D., Yu, M., Lou, Y., & Zhu, W. (2014). Production equation of fractured horizontal well in a water-bearing tight gas reservoir with low-velocity non-Darcy flow. *Journal of Natural Gas Science and Engineering*, *18*, 467-473.
[34] Fu, J., Su, Y., Li, L., Wang, W., Wang, C., & Li, D. (2022). Production model with mechanisms of multiple seepage in tight gas reservoir. *Journal of Petroleum Science and Engineering*, *209*, 109825.
[35] Lu, C., Qin, X., Ma, C., Yu, L., Geng, L., Bian, H., ... & Zhou, Y. (2022). Investigation of the impact of threshold pressure gradient on gas production from hydrate deposits. *Fuel*, *319*, 123569.
[36] Diwu, P., Liu, T., You, Z., Jiang, B., & Zhou, J. (2018). Effect of low velocity non-Darcy flow on pressure response in shale and tight oil reservoirs. *Fuel*, *216*, 398-406.